ON THE POSSIBILITY OF DESIGNING ANTI-REFLECTION COATINGS USING CHIRAL COMPOSITES

VIJAY K. VARADAN, VASUNDARA V. VARADAN and AKHLESH LAKHTAKIA
Research Center for the Engineering of Electronic and Acoustic Materials
Department of Engineering Science and Mechanics
The Pennsylvania State University
University Park, PA 16802

ABSTRACT

The possible use of chiral composite media for designing coatings instrumental in reducing EM reflection from metallic surfaces has been investigated. Such coatings may be fabricated by suspending chiral microgeometries in a dielectric matrix material. It is shown that these coatings can significantly cut down reflections, regardless of the incident polarization, over a wide frequency range (50-300 GHz) and incidence angles (0° - 30°).

1. INTRODUCTION

With the proliferation in the use of the electromagnetic spectrum at frequencies around 100 GHz witnessed by the past few years, it has become desirable to design efficient anti-reflection coatings for metallic surfaces. Low weight, low loss dielectric composites have been particularly attractive for this purpose, but such materials turn out to be poor absorbers of electromagnetic energy. There has been a need, therefore, to find materials which are lightweight but, in addition, are effective absorbers as well. The suspension of chiral microgeometries in such materials can endow them with what is called optical activity in physical chemistry, and it is the aim of this report to show that such materials are feasible for designing efficient anti-reflection coatings.

Ever since the discovery of optical activity in the early 19th century, physicists, chemists and biologists have been fascinated by it [1] - [6]. Insofar as the natural optical activity is concerned, it can be deduced from experiments conducted on crystals as well as organic liquids, that its source lies in a chiral (handed) molecular or crystal structure. Thus, a chiral substance might exist in two distinct molecular forms, which are otherwise identical in their chemical and physical properties; but although one is a mirror image of the other it cannot be superposed on its mirror image. In other words, the two molecules are incongruent mirror images of each other.

As might be readily supposed, most of the work has been done by physical chemists who have developed polarimetric techniques to investigate molecular and crystal structures. But chirality is a phenomenon which can be found in the less "exotic" everyday life. Möbius strips, golf clubs, helices, sea-shells, and, of course, the hands of a man (or, of a woman for that matter) are examples of chiral objects found everywhere. Substances with chiral microgeometries can, therefore, be tailored to possess desirable electromagnetic properties and their use exploited.

It will be shown in this report that chiral composites can be attractive as highly efficient absorbers. The electromagnetic boundary value problem of a plane chiral coating on a perfectly conducting surface will be investigated and several designs of such coatings discussed. From the numerical studies presented, it will be shown that endowing low loss dielectric composites with chiral properties can easily cut down the reflected power density by a factor of 4 or more.

2. CONSTITUTIVE AND WAVE EQUATIONS FOR THE CHIRAL MEDIUM

Consider a region V occupied by a chiral medium in which the usual constitutive relations $\underline{D} = \varepsilon\underline{E}$ and $\underline{B} = \mu\underline{H}$ do not hold due to their imcompatibility with the handedness of the medium. Instead, the relations

$$\underline{D} = \varepsilon\underline{E} + \alpha\varepsilon\nabla\times\underline{E} \quad , \quad \underline{B} = \mu\underline{H} + \beta\mu\nabla\times\underline{H} \tag{1}$$

hold, and have been seen to be sufficient enough to describe optical activity [2] - [6] via the parameters α and β. Use of the regular Maxwell's equations

$$\begin{aligned} \nabla\times\underline{E} &= i\omega\underline{E} \qquad & \nabla\cdot\underline{B} &= 0 \\ \nabla\times\underline{H} &= -i\omega\underline{D} \qquad & \nabla\cdot\underline{D} &= 0 \end{aligned} \tag{2}$$

is now made along with (1) to obtain the wave equation

$$\nabla^2\begin{pmatrix}\underline{E}\\ \underline{H}\end{pmatrix} = [K]^2\begin{pmatrix}\underline{E}\\ \underline{H}\end{pmatrix} \quad , \tag{3}$$

where the matrix K is given by

$$[K] = \frac{1}{1-k^2\alpha\beta}\begin{bmatrix} k^2\beta & i\omega\mu \\ -i\omega\varepsilon & k^2\alpha \end{bmatrix} \tag{4a}$$

with

$$k = \omega\sqrt{\mu\varepsilon} \quad , \tag{4b}$$

and an $\exp(-i\omega t)$ time dependence has been assumed. The fields $\underline{E}$ and $\underline{H}$ in V must also satisfy the auxiliary conditions

$$\nabla\times\begin{pmatrix}\underline{E}\\ \underline{H}\end{pmatrix} = [K]\begin{pmatrix}\underline{E}\\ \underline{H}\end{pmatrix} \quad ; \quad \nabla\cdot\begin{pmatrix}\underline{E}\\ \underline{H}\end{pmatrix} = \begin{pmatrix}0\\ 0\end{pmatrix} \tag{5}$$

along with (3).

Following Bohren [2], the electromagnetic field is transformed to

$$\begin{pmatrix}\underline{E}\\ \underline{H}\end{pmatrix} = [A]\begin{pmatrix}\underline{Q}_L\\ \underline{Q}_R\end{pmatrix} \tag{6}$$

where the left- and the right-handed fields, $\underline{Q}_L$ and $\underline{Q}_R$, respectively, must satisfy

$$\nabla^2\begin{pmatrix}\underline{Q}_L\\ \underline{Q}_R\end{pmatrix} + \begin{pmatrix}k_L^2 & \underline{Q}_L\\ k_R^2 & \underline{Q}_R\end{pmatrix} = 0 \tag{7}$$

along with

$$\nabla\times\begin{pmatrix}\underline{Q}_L\\ \underline{Q}_R\end{pmatrix} = \begin{pmatrix}k_L & \underline{Q}_L\\ -k_R & \underline{Q}_R\end{pmatrix} \quad , \quad \nabla\cdot\begin{pmatrix}\underline{Q}_L\\ \underline{Q}_R\end{pmatrix} = \begin{pmatrix}0\\ 0\end{pmatrix} \quad . \tag{8}$$

In (6) - (8), the matrix

$$[A] = \begin{bmatrix} 1 & a_R \\ a_L & 1 \end{bmatrix} , \tag{9a}$$

while

$$a_R = [k_R (1 - k^2\alpha\beta) + \alpha k^2] / j\omega\varepsilon \quad , \tag{9b}$$

$$a_L = [k_L (1 - k^2\alpha\beta) - \beta k^2] / j\omega\mu \quad , \tag{9c}$$

$$k_R = k \left\{ \left[1 + (\alpha - \beta)^2 k^2 / 4 \right]^{1/2} - (\alpha + \beta)k / 2 \right\} \left[1 - k^2\alpha\beta \right]^{-1} \quad , \tag{9d}$$

and

$$k_L = k \left\{ \left[1 + (\alpha - \beta)^2 k^2 / 4 \right]^{1/2} + (\alpha + \beta)k / 2 \right\} \left[1 - k^2\alpha\beta \right]^{-1} \quad . \tag{9e}$$

Thus, the electromagnetic field in V is given by

$$\underline{E} = \underline{Q}_L + a_R \underline{Q}_R \quad , \quad \underline{H} = a_L \underline{Q}_L + \underline{Q}_R \quad . \tag{10}$$

3. THE ANTI-REFLECTION COATING ON A METALLIC SURFACE

Let V be the region $0 \le z \le d$ occupied by a chiral medium whose properties are described above, and V′ be the half-space $z \le 0$ which does not exhibit chirality. The plane $z = d$ is assumed to be perfectly conducting so that the presented geometry describes a metallic surface coated with a chiral layer of thickness d. The primed quantities refer to the achiral half space V′, whereas the unprimed quantities hold in the layer V.

Consider a plane monochromatic wave

$$\underline{E}_i = (A_E \hat{y} - A_H \cos\theta_o \hat{x} + A_H \sin\theta_o \hat{z}) \exp [ik' (\cos\theta_o z + \sin\theta_o x)] \tag{11a}$$

$$\underline{H}_i = (1 / i\omega\mu') \nabla \times \underline{E}_i \tag{11b}$$

be traveling in V′ towards the interface $z = 0$, making an angle θ_o with the z axis. In (11) $k' = \omega\sqrt{(\mu'\varepsilon')}$ is the wavenumber in the achiral material occupying V′; and whereas the coefficients $A_E \neq 0$, $A_H = 0$ refer to a TE-polarized incident planewave, the coefficients $A_E = 0$, $A_H \neq 0$ denote an incident TM-polarized field.

Inside the chiral layer V, the existing field has to be expressed in terms of the solutions of (7) and (8), the $\underline{Q}_R$ denoting right-circularly polarized (RCP) waves and $\underline{Q}_L$, the left-circularly polarized (LCP) waves. One RCP and one LCP wave, in general, exist in V propagating towards $z = d$, and another pair of a LCP and a RCP wave propagating towards $z = 0$. Thus, the appropriate representation of the field in V is given by

$$\begin{aligned} \underline{Q}_L = {} & A_1 (-\cos\theta_L \hat{x} - i\hat{y} + \sin\theta_L \hat{z}) \exp \left[ik_L (\cos\theta_L z + \sin\theta_L x) \right] \\ & + A_2 (\cos\theta_L \hat{x} - i\hat{y} + \sin\theta_L \hat{z}) \exp \left[- ik_L (\cos\theta_L z - \sin\theta_L x) \right] \end{aligned} \tag{12a}$$

and

$$\begin{aligned} \underline{Q}_R = {} & C_1 (-\cos\theta_R \hat{x} + i\hat{y} + \sin\theta_R \hat{z}) \exp \left[ik_R (\cos\theta_R z + \sin\theta_R x) \right] \\ & + C_2 (\cos\theta_R \hat{x} + i\hat{y} + \sin\theta_R \hat{z}) \exp \left[-ik_R (\cos\theta_R z - \sin\theta_R x) \right] \quad . \end{aligned} \tag{12b}$$

In this representation, the coefficients A_1, A_2, C_1, C_2 are as yet unknowns to be determined as solutions of the boundary value problem; the coefficients A_1, C_1 refer to the waves going out to $z = d$, while the remaining two to those going towards $z = 0$. As per (10), the field in the chiral region is given in terms of

(12) by

$$\underline{E}_{ch} = \underline{Q}_L + a_R \underline{Q}_R \quad , \quad \underline{H}_{ch} = a_L \underline{Q}_L + \underline{Q}_R \ . \tag{13}$$

Finally, the representation of the reflected field in V takes the form

$$\underline{E}_{ref} = \left[A_3(\cos\theta'\hat{x} - i\hat{y} + \sin\theta'\hat{z}) + C_3(\cos\theta'\hat{x} + i\hat{y} + \sin\theta'\hat{z})\right] \cdot$$

$$\cdot \exp\left[-ik'(\cos\theta' z - \sin\theta' x)\right] \tag{14a}$$

$$\underline{H}_{ref} = (1 / i\omega\mu') \nabla \times \underline{E}_{ref} \tag{14b}$$

so that the reflected field also consists of a LCP and a RCP wave.

In order to solve the boundary value problem, the usual boundary conditions

$$\begin{aligned}
\hat{x} \cdot \left[\underline{E}_i + \underline{E}_{ref} - \underline{E}_{ch}\right] &= 0 \ , \quad z = 0 \\
\hat{x} \cdot \left[\underline{H}_i + \underline{H}_{ref} - \underline{H}_{ch}\right] &= 0 \ , \quad z = 0 \\
\hat{y} \cdot \left[\underline{E}_i + \underline{E}_{ref} - \underline{E}_{ch}\right] &= 0 \ , \quad z = 0 \\
\hat{y} \cdot \left[\underline{H}_i + \underline{H}_{ref} - \underline{H}_{ch}\right] &= 0 \ , \quad z = 0 \\
\hat{x} \cdot \left[\underline{E}_{ch}\right] &= 0 \ , \quad z = d \\
\hat{y} \cdot \left[\underline{E}_{ch}\right] &= 0 \ , \quad z = d
\end{aligned} \tag{15}$$

are enforced on the expansions (11) - (14) resulting in a 6×6 matrix to be solved numerically for the coefficients A_j, C_j, (j = 1, 2, 3). Furthermore, the phase-matching of the fields at the achiral-chiral interface z = 0 leads to the Fresnel conditions

$$k' \sin\theta_o = k' \sin\theta' = k_L \sin\theta_L = k_R \sin\theta_R \ . \tag{16}$$

Finally, the total reflected power density in V′ is evaluated as

$$P_{ref} = (1/2)\sqrt{\varepsilon' / \mu'}\ \cos\theta_o \left\{2\left|A_3\right|^2 + 2\left|C_3\right|^2\right\} \tag{17}$$

whereas the incident power density is given by

$$P_i = \begin{cases} (1/2)\sqrt{\varepsilon' / \mu'}\ \cos\theta_o \left|A_E\right|^2 \ , & \text{TE incidence} \\ (1/2)\sqrt{\varepsilon' / \mu'}\ \cos\theta_o \left|A_H\right|^2 \ , & \text{TM incidence} \end{cases} \tag{18}$$

Computations of the reflection efficiencies

$$R = P_{ref} / P_i \tag{19}$$

can therefore be made. It must be noted that (1 – R) is the absorption efficiency of the chiral layer since whatever energy is not reflected back into V′ must have been absorbed in V. Furthermore, in order to guarantee the energy conservation principle in an otherwise lossless medium, the condition $\alpha = \beta^*$ in the constitutive equation (1) for the chiral medium is sufficient.

4. NUMERICAL RESULTS AND SOME COATING DESIGNS

With the theoretical framework for the anti-reflection chiral coating problem thus accomplished, it will be appropriate to discuss the numerical results obtained. The matrix equation resulting from (15) was programmed on a DEC VAX 11/730 minicomputer and the reflection efficiencies R_{TE}, R_{TM} of (19) were computed for both incident polarizations. The achiral half-space V′ was taken to be free-space so the $\varepsilon' = \varepsilon_o$

computed for both incident polarizations. The achiral half-space V′ was taken to be free-space so the $\varepsilon' = \varepsilon_o$ and $\mu' = \mu_o$. In addition, the chiral layer was taken to be devoid of magnetic properties and μ was set equal to μ_o. On the other hand, V was filled up by a low loss chiral dielectric medium so that its relative permittivity $\varepsilon/\varepsilon_o$ was complex with $\text{Im}\{\varepsilon/\varepsilon_o\} << \text{Re}\{\varepsilon/\varepsilon_o\}$. The thickness d of the coating was assumed to be 2 mm for all the numerical studies following.

In Fig. 1, the reflection efficiencies R_{TE} and R_{TM} are plotted as functions of the angle of incidence θ_o for (a) $\varepsilon/\varepsilon_o = 5.0 + i0.1$ and (b) $\varepsilon/\varepsilon_o = 5.0 + i0.05$. The frequency of the incident radiation is set at 100 GHz while $\beta = \alpha^*$ is varied. From this figure, it must be noted that for normal incidence, $R_{TE} = R_{TM}$, as may be verified by substituting $\theta_o = 0°$ in the equations of the preceding section. Furthermore, provided β is real, the reflection efficiencies are considerably lower than for an otherwise lossy dielectric achiral coating. On the other hand, taking β to be complex seems to serve no purpose in reducing reflection by the use of the handedness of the layer medium. In any case, $\beta = \alpha$ guarantees the time-reversal symmetry of the solution [6]; therefore, along with the condition $\beta = \alpha^*$ for energy conservation to hold [4], in all subsequent numerical studies presented $\beta = \alpha$ has been assumed to be real.

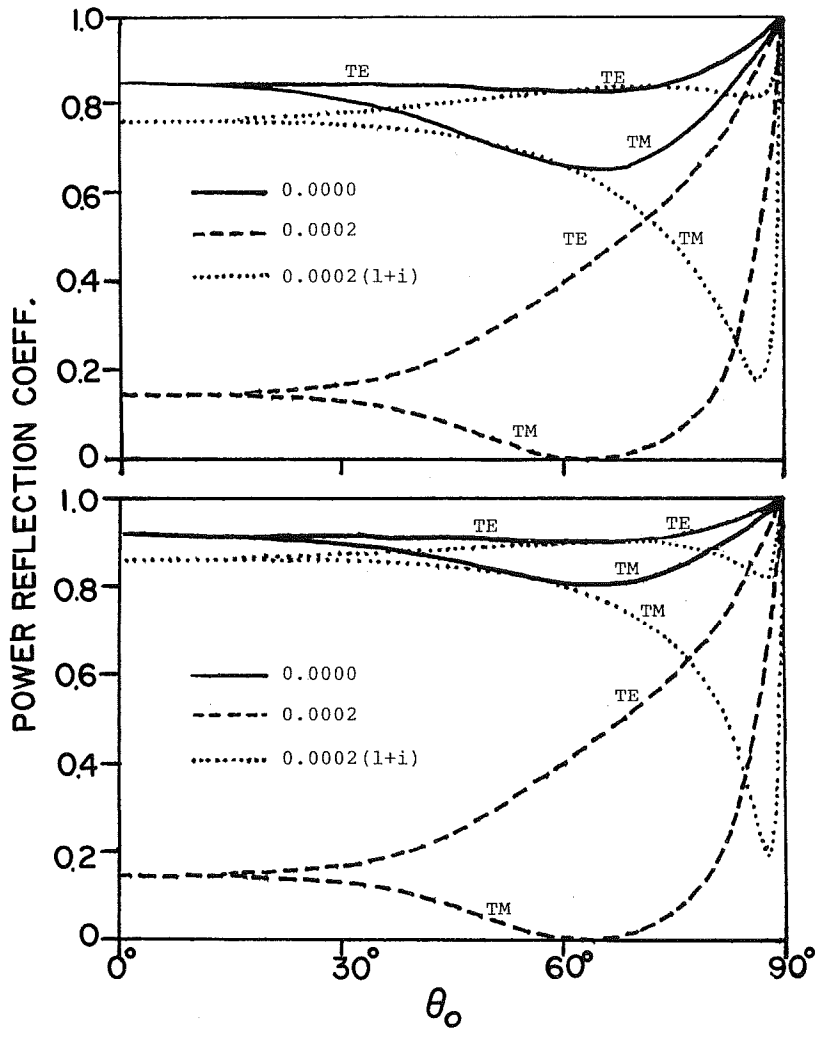

Figure 1 Reflection efficiencies R_{TE} and R_{TM} for a 2 mm thick chiral anti-reflection coating as a function of the incidence angle θ_o at a frequency of 100 GHz. (a) $\varepsilon/\varepsilon_o = 5.0 + i0.1$, (b) $\varepsilon/\varepsilon_o = 5.0 + i0.05$. The chiral parameter $\beta = \alpha^*$ is set at 0.0 m (achiral), 0.0002 m and 0.0002 (1 + i) m.

Next, in Fig. 2 R_{TE} and R_{TM} are again plotted with $\varepsilon/\varepsilon_0 = 5.0 + i0.05$ and $0° \leq \theta_0 \leq 90°$ at a frequency of 100 GHz. This time β is real and is varied from 0.0 (achiral lossy dielectric) to 0.0005 m. Clearly, it appears that for both TE and TM polarized incidence cases $\beta = 0.0002$ m is an optimum value for the reduction of the reflected energy in the zone $0° \leq \theta \leq 45°$.

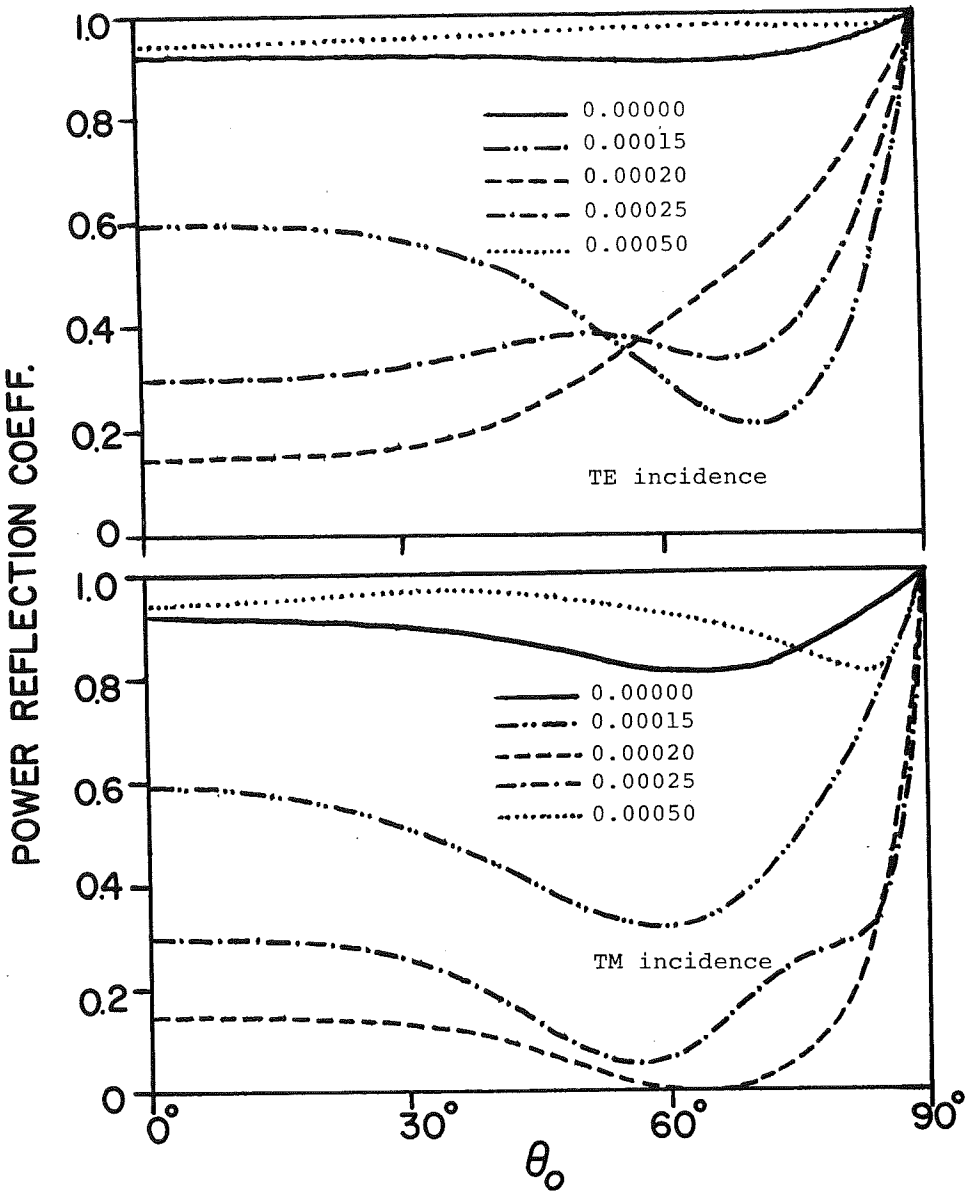

Figure 2 Reflection efficiencies R_{TE} and R_{TM} for a 2 mm thick chiral anti-reflection coating as a function of the incidence angle θ_0 at a frequency of 100 GHz. The relative permittivity $\varepsilon/\varepsilon_0 = 5.0 + i0.05$ while the chiral parameter β is varied from 0.0 m to 0.0005 m.

A design of a wideband anti-reflection chiral coating, however, cannot afford to have both $\varepsilon/\varepsilon_0$ and β independent of frequency. This can be observed from Fig. 3 where the 2 mm thick chiral coating has $\varepsilon/\varepsilon_0 = 5.0 + i0.05$ and $\beta = 0.0002$ m over the frequency range 50-300 GHz. The angle of incidence $\theta_0 = 15°$ and only R_{TE} is plotted. The various peaks must be noted in this figure and they refer to anomalies of the kind described by several authors for surface scattering problems [7]. Hence, the big anomaly marked at about 110 GHz when the plane of constant phase of the RCP wave in V tilts at a complex angle w.r.t. the z-axis.

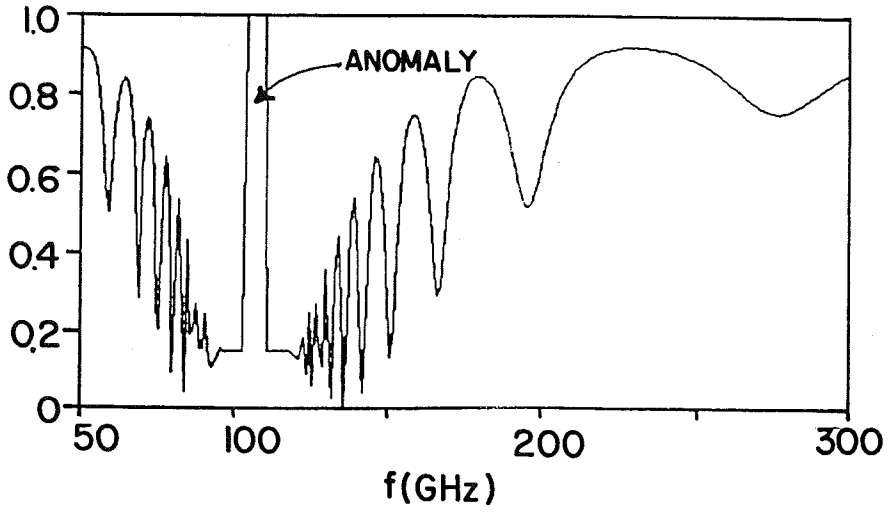

Figure 3 Reflection efficiency R_{TE} for a 2 mm thick chiral anti-reflection coating as a function of frequency when a planewave is incident on it at an angle $\theta_0 = 15°$. The parameters $\varepsilon/\varepsilon_0 = 5.0 + i0.05$ and $\beta = 0.0002$ m.

Once it becomes clear from numerical experimentation that (a) chirality is ineffective in the reduction of the reflection efficiency if $\varepsilon/\varepsilon_0$ is purely real, and (b) that either β or $\varepsilon/\varepsilon_0$ or both must be frequency dependent in order to obtain a wideband anti-reflection coating, design of such a coating becomes more of an optimization problem. In the first of such designs to be described here, $\beta = \beta(f)$ assumed is shown in Fig. 4.

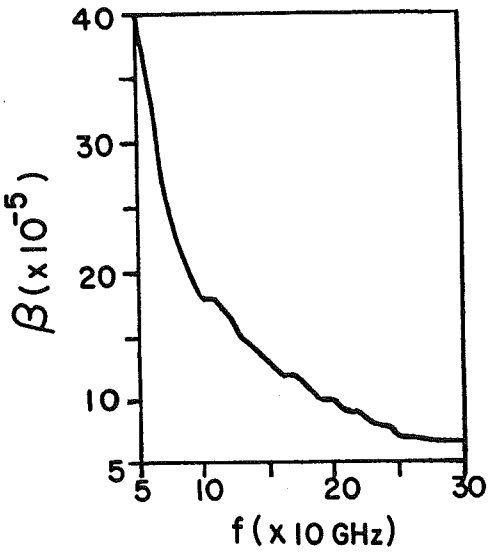

Figure 4 The frequency profile $\beta = \beta(f)$ used for the results shown in Figs. 5 and 6. The parameter β carries the unit of meter.

In Figs. 5 and 6, the enhancement of the absorption efficiency of over a 50-300 GHz frequency range by incorporating this frequency dependent $\beta = \beta(f)$ is illustrated, for the TE- and TM- polarization incidence cases, respectively. The relative permittivity $\varepsilon/\varepsilon_o$ is set at 5.0 + i0.05 for all frequencies considered. It should be noted from these two figures that whereas the design objective of achieving R_{TE} and R_{TM} less than 20% for $50 \leq f \leq 300$ GHz and $0° \leq \theta_o \leq 30°$ can be achieved using the β of Fig. 4, the reflection efficiences hover around 92% if β were to be set equal to zero.

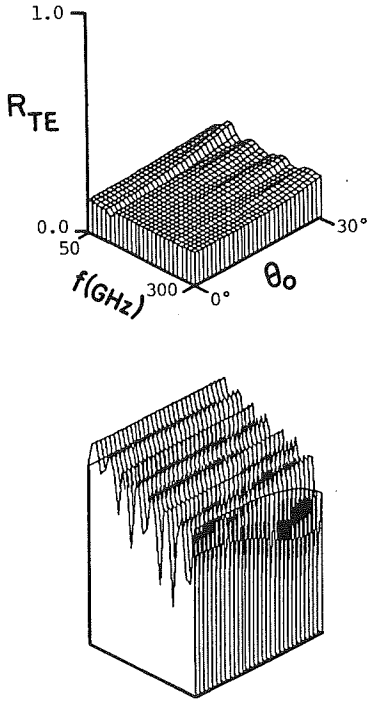

Figure 5 Reflection efficiency R_{TE} plotted as a function of θ_o and frequency f for a 2 mm thick anti-reflection coating. The complex permittivity $\varepsilon/\varepsilon_o = 5.0 + i0.05$. In the upper figure the $\beta = \beta(f)$ of Fig. 4 is used while in the lower figure β is set equal to 0.0 m.

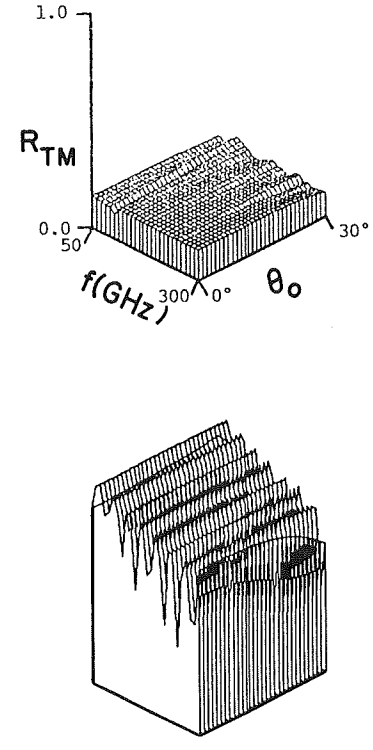

Figure 6 Same as Fig. 5, but R_{TM} is plotted.

The design objectives for Figs. 7-9 were slightly modified. No more than a reflection efficiency of 25% was to be tolerated over the frequency range of 50-300 GHz with the angle of incidence varying from 0° to 30°. This goal should also be met regardless of the polarization of the incident planewave. The chirality

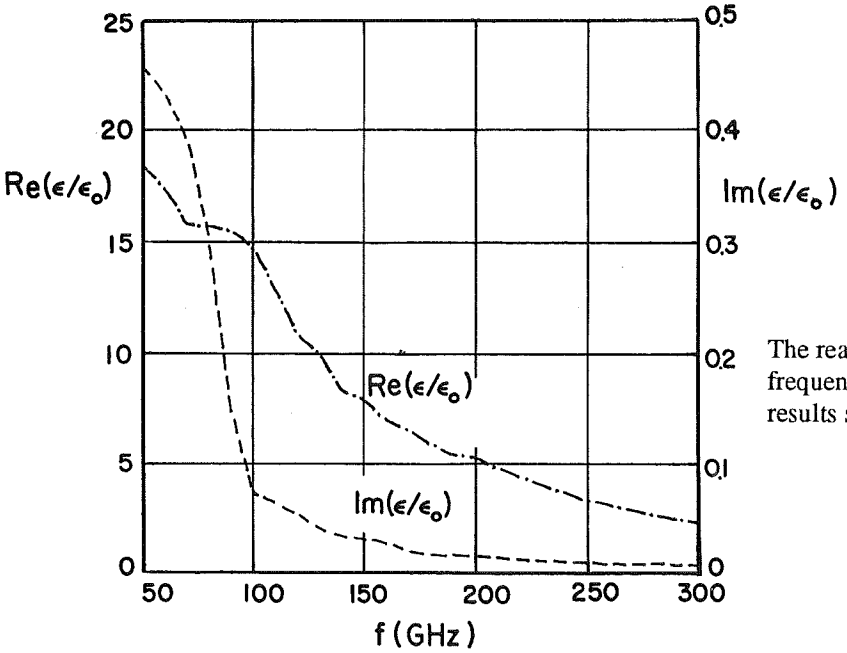

Figure 7
The real and the imaginary parts of the frequency dependent $\varepsilon/\varepsilon_0$ used for the results shown in Figs. 8 and 9.

parameter $\beta = 0.0001$ m while $\varepsilon/\varepsilon_0$ could be varied over the frequency range. The designed frequency profile of $\varepsilon/\varepsilon_0$ is shown in Fig. 7, while from Figs. 8 and 9 it can be inferred that this goal was successfully met. It should be mentioned here that at no frequency in the desired range did the loss factor tan δ of the chiral layer exceed 0.025, thereby showing that the incorporation of chirality in an otherwise low loss dielectric coating turns it into a highly absorbing layer.

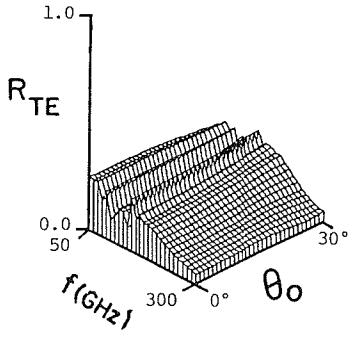

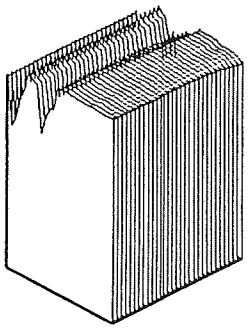

Figure 8 Reflection efficiency R_{TE} plotted as a function of θ_0 and frequency f for a 2 mm thick anti-reflection coating. The values of $\varepsilon/\varepsilon_0$ are taken from Fig. 7, and whereas the upper figure has $\beta = 0.0002$ m, the lower figure assumes $\beta = 0.0$ m.

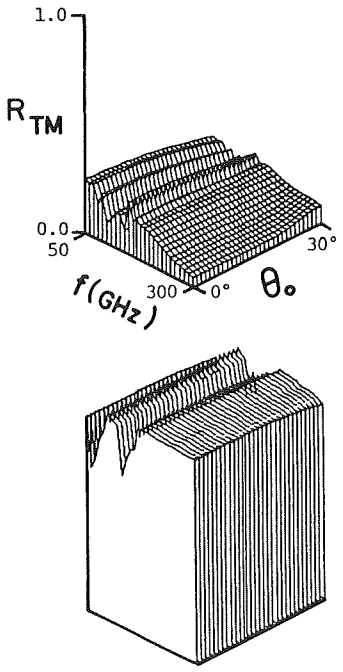

Figure 9 Same as Fig. 8, but R_{TM} is plotted.

Yet another design fulfilling the objectives of this problem is shown in Fig. 10 where β has been set constant at 0.000125 m, while tan δ of V does not exceed 0.015. Finally, in Fig. 11 even a larger value 0.0002 m of β has been used but the bandwidth has been reduced to 50-200 GHz.

From the preceding four design problems several conclusions can be drawn. Firstly, in reducing reflection if a larger constant β is used, then the values of $\varepsilon/\varepsilon_0$ tend to decrease over the entire frequency band of interest, a goal which appears to be desirable for a material scientist. However, this also tends to reduce the bandwidth over which the desired absorption efficiencies can be achieved.

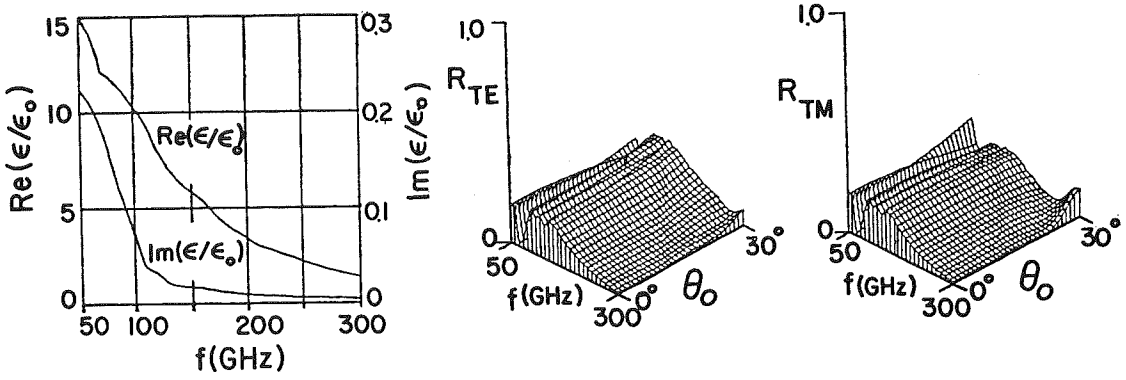

Figure 10 The assumed frequency profile of $\varepsilon/\varepsilon_0$ for a 2 mm thick anti-reflection coating is shown. The reflection efficiencies R_{TE} and R_{TM} are plotted as functions of θ_0 and the frequency f, with the chirality parameter β = 0.000125 m.

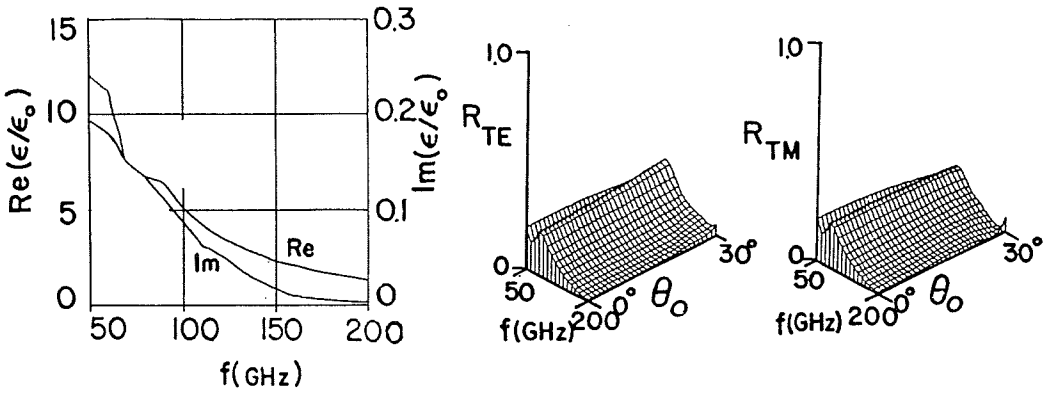

Figure 11 Same as Fig. 10, but with $\beta = 0.0002$ m.

Secondly, and as stated earlier, chirality in the absence of a lossy ε is of no use whatsoever in reducing reflected power density. A small loss must be present for ε to be effective. Therefore, chirality serves only as an enhancement factor for absorption, but of itself it is not an absorbing mechanism. Thirdly, and very importantly, both $\varepsilon/\varepsilon_0$ and β should be frequency dependent. This last conclusion, however, was not verified here because of the complexities of multivariate optimization problems.

5. CONCLUSION

In summary, this report describes the use of low loss dielectric chiral composites to fabricate low weight and highly effective anti-reflection coatings. Low loss dielectrics in the ~100 GHz frequency range of this kind are quite commonly available and are attractive because of their low mass densities. However, such materials are not very effective absorbers. Suspension of chiral microgeometries in these materials can, however, endow them with rotational activity, and simultaneously, turn them into efficient absorbers of electromagnetic radiation.

REFERENCES

1. L.D. Barron, *Molecular Light Scattering and Optical Activity,* Cambridge University Press, Cambridge, Great Britain (1982).

2. C.F. Bohren, Light Scattering by an Optically Active Sphere, *Chem. Phys. Lett.* **29**, 458-462 (1974).

3. C.F. Bohren, Scattering of Electromagnetic Waves by an Optically Active Cylinder, *J. Coll. Interface Sci.* **66**, 105-109 (1978).

4. F.I. Fedorov, On the Theory of Optical Activity in Crystals, I. The Law of Conservation of Energy and the Optical Activity Tensors, *Opt. Spectrosc.* (USSR) **6**, 49-53 (1959),

5. B.V. Bokut' and F.I. Fedorov, On the Theory of Optical Activity in Crystals, III. General Equation of Normals, *Opt. Spectrosc.* (USSR) **6**, 342-344 (1959).

6. R.A. Satten, Time-reversal Symmetry and Electromagnetic Polarization Fields, *J. Chem. Phys.* **28**, 742-743 (1958).

7. S.L. Chuang and J.A.Kong, Scattering of Waves from Periodic Surfaces, *Proc. IEEE* **66**, 1132-1144 (1981).